

SADA: Semantic Adversarial Diagnostic Attacks for Autonomous Applications

Abdullah Hamdi, Matthias Müller, Bernard Ghanem

King Abdullah University of Science and Technology (KAUST), Thuwal, Saudi Arabia

{abdullah.hamdi, matthias.mueller.2, bernard.ghanem}@kaust.edu.sa

Abstract

One major factor impeding more widespread adoption of deep neural networks (DNNs) is their issues with robustness, which is essential for safety critical applications such as autonomous driving. This has motivated much recent work on adversarial attacks for DNNs, which mostly focus on pixel-level perturbations void of semantic meaning. In contrast, we present a general framework for adversarial black box attacks on agents, which are intimately related to the semantics of the task being performed by the agent. To do this, our proposed adversary (denoted as BBGAN) is trained to appropriately parametrize the environment (black box) with which the agent interacts, such that this agent performs poorly on its dedicated task. We illustrate the application of our BBGAN framework on three different tasks (primarily targeting aspects of autonomous navigation): object detection, self-driving, and autonomous UAV racing. On these tasks, our approach can be used to generate failure cases that fool an agent consistently.

1. Introduction

As a result of recent advances in machine learning and computer vision, deep neural networks (DNNs) are now interleaved with many aspects of our daily lives. DNNs are used to suggest news articles to read and movies to watch, automatically edit our photos and videos, and translate between hundreds of languages. Deep neural networks are also bound to disrupt transportation with autonomous driving slowly becoming a reality. However, while there are already impressive demos and some successful deployments, safety concerns for boundary conditions persist. While current models work very well on average, they struggle with robustness in certain cases.

Recent work in the adversarial attack literature shows how sensitive DNNs are to input noise. These attacks usually utilize the information about the network structure to perform gradient updates in order to derive targeted perturbations. These perturbations are injected into the input image at the pixel-level, so as to either confuse the network or enforce a specific behavior [47, 19, 9, 27]. There are also attacks that assume the DNN to be a black box, but they still

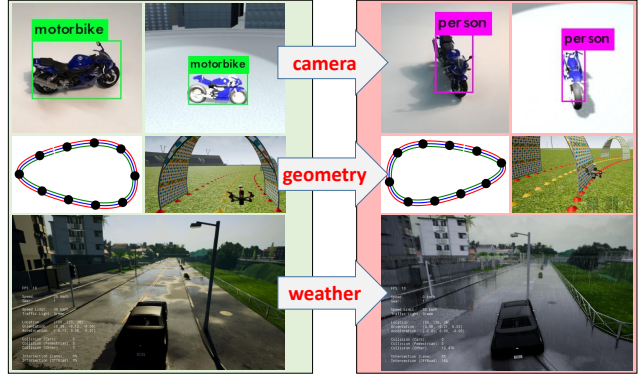


Figure 1: **Semantic Adversarial Diagnostic Attacks.** Neural networks can perform very well on average for a host of tasks; however, they do perform poorly or downright fail when encountering some environments. To diagnose why they fail and how they can be improved, we seek to learn the underlying distribution of semantic parameters, which generate environments that pose difficulty to these networks when applied to three safety critical tasks: object detection, self-driving cars, and autonomous UAV racing.

operate at the pixel-level [12, 36]. Targeted pixel attacks can lead to severe performance drop not only on classification, but also on tasks like object detection [13], face recognition [45], speech recognition [10], and segmentation [52].

In practice, such pixel attacks are much less likely to naturally occur than semantic attacks, including changes in camera viewpoint, lighting conditions, street layouts, etc. The literature on semantic attacks is much sparser, since they are much more subtle and difficult to analyze [55]. Yet, this type of attack is critical to understand/diagnose failure cases that might occur in the real-world. While it is very difficult to investigate semantic attacks on real data, we can leverage simulation as a proxy that can unearth useful insights transferable to the real-world. Figure 1 shows an example of an autonomous driving failure case in a popular driving simulator (CARLA [15]), an object misclassification by YOLOV3 [40] applied to an image generated by Blender [7], and an autonomous UAV racing [34] failure case in a recently developed general purpose simulator (Sim4CV [33]). These failures arise from adversarial attacks on the semantic parameters generating the simula-

tion/rendering environment.

In this work, we consider environments that are adequately photo-realistic and parameterized by a compact set of variables that have direct semantic meaning (*e.g.* camera viewpoint, lighting/weather conditions, road layout, etc.). Since the generation process of these environments from their parameters is quite complicated and in general non-differentiable, we treat it as a *black box* function. We seek to learn an adversary that can produce fooling parameters that construct an environment, in which the agent (which is also a black box) fails in its task. Unlike most adversarial attacks that generate sparse instances of failure, our proposed adversary should provide a more comprehensive view on how an agent can fail by learning to sample from the distribution of fooling parameters for a particular agent and task. Since Generative Adversarial Networks (GANs [18, 3]) have emerged as a promising family of unsupervised learning techniques that can model complicated distributions [54, 23, 22, 28], we propose to model our adversary as a GAN, denoted appropriately as black-box GAN (BBGAN).

Contributions. (1) We formalize adversarial attacks in a more general setup to include both semantic and conventional pixel adversarial attacks. (2) We propose BBGAN in order to learn the underlying distribution of semantic adversarial attacks. (3) We show promising results on three different safety-critical applications used in autonomous navigation, thus, illustrating the usefulness of our approach in analyzing the agent failure, along with some analysis and insights about transferability of these attacks.

2. Related Work

Attacks on Classifiers by Pixel Perturbation. The work of Szegedy [47] was the first to introduce a formulation of attacking neural networks as an optimization. The method minimizes the perturbation of the image pixels, while still fooling a trained classifier to predict a wrong class label. Several works followed the same approach but with different formulations, such as Fast Gradient Sign Method (FGSM) [19] and Projected Gradient Descent [27, 32]. The notable work of Carlini and Wagner [9] performs a comprehensive study of different losses and ways to fool the network with minimal pixel perturbation. As an alternative to pixel attacks, recent work by Hosseini and Poovendran [21] investigates color shifting. Several works have shown how these attacks can be transferred to the real-world by printing perturbed images on paper [26] or building 3D objects based on fooling images [4]. However, all these methods are limited to pixel perturbations and only fool classifiers, while we consider more general cases of attacks, *e.g.* changes in camera viewpoint to fool a detector or change in weather conditions to fool a self-driving car.

Most of these attacks are white-box attacks, in which the algorithm has access to network gradients. Dezfooli

et al. [31] introduce a universal attack that works well on networks that are not used in training the adversary. The work of Chen *et al.* [12] develops a black box attack by only assuming access to the output of the classifier. Since back-propagation cannot be performed, the gradient is approximated by finite differences instead. Bhagoji *et al.* [36] perform a black-box attack with a small number of network queries by using PCA and randomized dimension selection in the gradient estimation step. While we assume black box constraints in our work, we are interested in the distribution of the semantic parameters that fool the agent, more so than individual fooling examples. This limits the usefulness of approximating the gradient to reach a single local solution.

Attacks beyond Classifiers. Sharif *et al.* [45] demonstrate attacks on other perception networks and attack a face recognition system by painting frames of sunglasses. Calini and Vagner use adversarial attacks to confuse a speech recognition system [10]. Xie *et al.* [52] perform adversarial attacks on object detection and segmentation by perturbing image pixels and show the transferability of the perturbation to different networks. Chen *et al.* [13] propose expectation over transformation to construct adversarial attacks on faster R-CNN [41] that is robust to perspective and occlusion. However, they only demonstrate how it works on stop-signs.

Attacks beyond Pixels. Moving away from pixel perturbation to semantic 3D scene parameters, Zeng *et al.* [55] generate attacks on deep classifiers and Visual Question and Answering agents by perturbing scene parameters like lighting and surface normals. They show that most common image space adversarial attacks are not authentic and cannot be realized in real 3D scenes. Inspired by this insight, we tackle this issue by using readily available virtual environments with plausible 3D setups to test the agents more systematically. In fact, our formulation includes attacks not only on static agents like object detectors, but also agents that interact with updating environments, such as self-driving agents. To the best of our knowledge, this is the first work to introduce adversarial attacks in CARLA [15], a standard autonomous navigation benchmark.

Generic Adversarial Attacks/Reinforcement Learning.

We formulate black-box adversarial attacks in a general setup that includes an environment and agent. An adversary suggests fooling parameters to the environment, then the agent receives an observation from the environment and produces an action. The environment then scores the agent and updates its state until the episode finishes. The adversary uses the final score from the environment during training to update its next attack. This general setup includes both pixel perturbation attacks as well as semantic attacks. This formulation is naturally inspired by Reinforcement Learning (RL), in which agents can have multiple actions and receive partial rewards as they proceed in their task [46]. However, in RL, the agent is the focus of learning

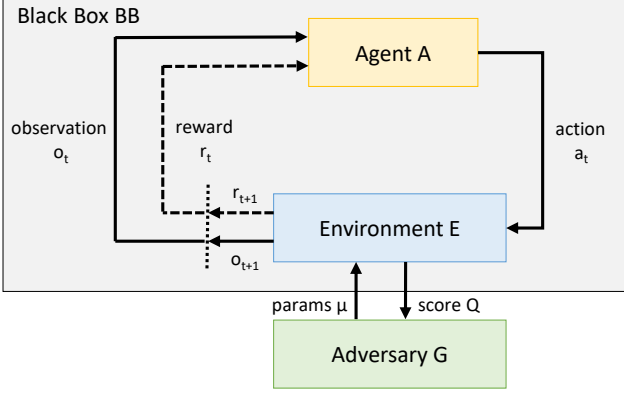


Figure 2: **Generic Adversarial Attacks on Agents.** \mathbf{E}_μ is a parametric environment that an agent \mathbf{A} lives in, where the agent receives an observation \mathbf{o}_t from the environment and produces an action \mathbf{a}_t , and then the environment would score the agent and update its state until the episode finishes. After that, a final score $Q(\mathbf{A}, \mathbf{E}_\mu)$ is given for the adversary \mathbf{G} that proposes the input parameters μ , so it can update itself and proposes a stronger attack for the next iteration.

and the goal is to achieve a task in the environment. In contrast, in adversarial attacks, the agent is usually fixed and learning is performed by the adversary in order to fool the agent or diagnose it. Recent work in [53] introduces an RL environment update as a way to improve the performance of agents inside this environment. In contrast, our virtual environment is parameterized by semantic attributes with the goal of fooling and analyzing the already trained agent.

3. Methodology

Typical adversarial pixel attacks involve a neural network agent \mathbf{C} (e.g. classifier or detector) that takes an image $\mathbf{x} \in [0, 1]^n$ as input and outputs a multinoulli distribution over K class labels with softmax values $[l_1, l_2, \dots, l_K]$, where l_j is the softmax value for class j . The adversary (attacker) tries to produce a perturbed image $\mathbf{x}' \in [0, 1]^n$ that is as close as possible to \mathbf{x} and where $\mathbf{C}(\mathbf{x}) \neq \mathbf{C}(\mathbf{x}')$. The objective to be optimized can be formulated as follows:

$$\min_{\mathbf{x}'} d(\mathbf{x}, \mathbf{x}') \quad \text{s.t. } \mathbf{C}(\mathbf{x}) \neq \mathbf{C}(\mathbf{x}'); \mathbf{x}' \in [0, 1]^n \quad (1)$$

where $d(\mathbf{x}, \mathbf{x}')$ is the distance, e.g. $\|\mathbf{x} - \mathbf{x}'\|_2$ or $\|\mathbf{x} - \mathbf{x}'\|_\infty$.

3.1. Generalizing Adversarial Attacks

Extending attacks to general agents. In this work, we generalize the adversarial attack setup beyond pixel perturbation attacks. Our more general setup (refer to Figure 2) includes semantic attacks, e.g. perturbing the camera pose or lighting conditions of the environment that generates observations (e.g. pixels of 2D images). In this setup, an environment \mathbf{E}_μ is parametrized by $\mu \in [\mu_{\min}, \mu_{\max}]^d$. It

has an internal state \mathbf{s}_t and produces observations $\mathbf{o}_t \in \mathbb{R}^n$ at each time step $t \in \{1, \dots, T\}$. The environment interacts with a trained agent \mathbf{A} , which takes observations \mathbf{o}_t from the environment to produce actions \mathbf{a}_t . At each time step t and after the agent performs an action \mathbf{a}_t , the internal state of the environment is updated with $\mathbf{s}_{t+1} = \mathbf{E}_\mu(\mathbf{s}_t, \mathbf{a}_t)$. The environment rewards the agent with $r_t = R(\mathbf{s}_t, \mathbf{a}_t)$, for some reward function R . We define the episode score $Q(\mathbf{A}, \mathbf{E}_\mu) = \sum_{t=1}^T r_t$ of all intermediate rewards. The goal of agent \mathbf{A} is to complete a task by maximizing Q . Outside the black box (environment and agent), the adversary \mathbf{G} tries to attack \mathbf{A} by modifying the environment through its parameters μ .

Distribution of Adversarial Attacks. We define $\mathbf{P}_{\mu'}$ to be the *fooling distribution* of semantic parameters μ' representing environment $\mathbf{E}_{\mu'}$, which fools agent \mathbf{A} . Formally, it is defined as follows:

$$\mu' \sim \mathbf{P}_{\mu'} \Leftrightarrow Q(\mathbf{A}, \mathbf{E}_{\mu'}) \leq \epsilon; \mu' \in [\mu_{\min}, \mu_{\max}]^d \quad (2)$$

where ϵ is a small threshold that is defined for each specific adversarial attack. Distribution $\mathbf{P}_{\mu'}$ ensures both exploration and exploitation, since it covers all failure cases of \mathbf{A} and still results in successful attacks for all of its samples. Hence, we seek an adversary \mathbf{G} that tries to learn $\mathbf{P}_{\mu'}$, so it can be used to comprehensively analyze the weaknesses of \mathbf{A} . Unlike the common practice of finding individual adversarial examples (most often images), we address the attacks distribution-wise and in a compact semantic parameter space describing the environment. We denote our analysis technique as Semantic Adversarial Diagnostic Attack (SADA): *semantic* because of the nature of the parameters representing the environment and *diagnostic* because a fooling distribution is sought. In Section 5.4, we highlight what such semantic attacks can reveal about the nature of the agents used in safety-critical tasks like object detection and self-driving.

For the adversary \mathbf{G} to achieve this challenging goal, we propose to optimize the following objective:

$$\begin{aligned} \arg \min_{\mathbf{G}} \mathbb{E}_{\mu \sim \mathbf{G}} [Q(\mathbf{A}, \mathbf{E}_\mu)] \\ \text{s.t. } \{\mu : \mu \sim \mathbf{G}\} = \{\mu' : \mu' \sim \mathbf{P}_{\mu'}\} \end{aligned} \quad (3)$$

Algorithm 1 describes a general setup for the adversary \mathbf{G} to learn to generate fooling parameters. It also includes a mechanism for evaluating \mathbf{G} after training it to attack agent \mathbf{A} in the black box environment \mathbf{E}_μ for N iterations. An attack is considered a fooling attack, if parameter μ sampled from \mathbf{G} achieves an episode score $Q(\mathbf{A}, \mathbf{E}_\mu) \leq \epsilon$. Consequently, the Attack Fooling Rate (AFR) is defined as the rate at which samples from \mathbf{G} are fooling attacks. In addition to AFR, the algorithm returns the set $\mathcal{S}_{\mu'}$ of adversarial examples that can be used to diagnose the agent. The equality constraint in Eq (3) is very strict to include *all* the fooling parameters μ' in the learned fooling distribution. It

Algorithm 1: Generic Adversarial Attacks on Agents

Requires: Adversary \mathbf{G} , Environment \mathbf{E}_μ , Agent \mathbf{A} , number of episodes T , training iterations N , test size M

Training \mathbf{G} :

```
for  $i \leftarrow 1$  to  $N$  do
  sample parameter vector  $\mu_i$  from  $\mathbf{G}$ 
  Initialize  $E_{\mu_i}$  with initial state  $s_1$ 
  for  $t \leftarrow 1$  to  $T$  do
     $E_{\mu_i}$  produces observation  $\mathbf{o}_t$  from  $s_t$ 
     $\mathbf{A}$  produces an action  $\mathbf{a}_t$  given observation  $\mathbf{o}_t$ 
     $E_{\mu_i}$  rewards  $\mathbf{A}$  with  $r_t = R(s_t, \mathbf{a}_t)$ 
     $E_{\mu_i}$  updates its internal state to  $s_{t+1} = E_{\mu_i}(s_t, \mathbf{a}_t)$ 
  end
   $\mathbf{G}$  receives the episode score  $Q_i(\mathbf{A}, \mathbf{E}_\mu) = \sum_{t=1}^T r_t$ 
  update  $\mathbf{G}$  to solve for Eq (3)
end
```

Testing \mathbf{G} :

```
Initialize: foolingCounter = 0 ;  $S_{\mu'} = \{\}$ 
for  $j \leftarrow 1$  to  $M$  do
  sample parameter vector  $\mu_j$  from  $\mathbf{G}$ 
  Initialize  $E_{\mu_j}$  with initial state  $s_1$ 
  for  $t \leftarrow 1$  to  $T$  do
     $r_t = R(s_t, \mathbf{a}_t)$  ;  $s_{t+1} = E_{\mu_j}(s_t, \mathbf{a}_t)$ 
     $Q_j(\mathbf{A}, \mathbf{E}_{\mu_j}) = \sum_{t=1}^T r_t$ 
  end
  if  $Q_j(\mathbf{A}, \mathbf{E}_{\mu_j}) \leq \epsilon$  then
    Fool attacks  $\mathbf{A}$ :  $S_{\mu'} \leftarrow S_{\mu'} \cup \{\mu_j\}$ 
    foolingCounter  $\leftarrow$  foolingCounter + 1
  end
end
```

foolingRate = foolingCounter/ M

Returns: foolingRate, $S_{\mu'}$

acts as a perceptuality metric in our new generalized attack to prevent unrealistic attacks. However, since this is very difficult, we relax the equality constraint in Eq (3). In the following section we propose to leverage DNNs and recent advances in generative models to learn an estimate of the distribution $\mathbf{P}_{\mu'}$.

3.2. Black Box Generative Adversarial Network

Generative Adversarial Networks (GANs) are a promising family of unsupervised techniques that can model complex domains, e.g. natural images [18, 3, 20]. GANs consist of a Discriminator \mathbf{D}_x and a Generator \mathbf{G}_x that are adversarially trained to optimize the loss $L_{GAN}(\mathbf{G}_x, \mathbf{D}_x, \mathbf{P}_X)$.

$$\min_{\mathbf{G}_x} \max_{\mathbf{D}_x} L_{GAN}(\mathbf{G}_x, \mathbf{D}_x, \mathbf{P}_X) = \mathbb{E}_{\mathbf{x} \sim p_x(\mathbf{x})} [\log \mathbf{D}_x(\mathbf{x})] + \mathbb{E}_{\mathbf{z} \sim p_z(\mathbf{z})} [\log(1 - \mathbf{D}_x(\mathbf{G}_x(\mathbf{z})))] \quad (4)$$

where \mathbf{P}_X is the distribution of images in domain X and $\mathbf{z} \in \mathbb{R}^c$ is a latent random Gaussian vector. \mathbf{D}_x tries to determine if a given sample (e.g. image \mathbf{x}) is real (from training) or fake (generated by \mathbf{G}_x). On the other hand, \mathbf{G}_x tries to randomly generate samples that better fool \mathbf{D}_x (e.g. mis-

classification). Both networks are proven to converge when \mathbf{G}_x can reliably produce the underlying distribution of the real samples [18].

In this paper, we propose to learn the fooling distribution $\mathbf{P}_{\mu'}$ using a GAN setup, which we denote as black box GAN (BBGAN). We follow the same GAN objective, as in Eq (4), while replacing the image domain \mathbf{x} by the semantic environment parameter μ . However, since we do not have direct and ready access to $\mathbf{P}_{\mu'}$ (i.e. no *real* environment parameters), we propose a module called the *inducer*, which is tasked to produce a plausible parameter set $S_{\mu'}$ that belongs to $\mathbf{P}_{\mu'}$. This setup translates into the relaxation of the problem in Eq (3) to:

$$\begin{aligned} & \arg \min_{\mathbf{G}} \mathbb{E}_{\mu \sim \mathbf{G}} [Q(\mathbf{A}, \mathbf{E}_\mu)] \\ & \text{s.t. } \{\mu : \mu \sim \mathbf{G}\} \subset \{\mu' : \mu' \sim \mathbf{P}_{\mu'}\} \end{aligned} \quad (5)$$

So, the final BBGAN loss is as follows.

$$\begin{aligned} & \min_{\mathbf{G}_\mu} \max_{\mathbf{D}_\mu} L_{BBGAN}(\mathbf{G}_\mu, \mathbf{D}_\mu, S_{\mu'}) = \\ & \mathbb{E}_{\mu \sim S_{\mu'}} [\log \mathbf{D}_\mu(\mu)] + \mathbb{E}_{\mathbf{z} \sim p_z(\mathbf{z})} [\log(1 - \mathbf{D}(\mathbf{G}(\mathbf{z})))] \end{aligned} \quad (6)$$

Here, \mathbf{G}_μ is the generator and acts as the adversary, and $\mathbf{z} \in \mathbb{R}^m$ is a random variable sampled from a normal distribution. A simple inducer can be just a filter that uniformly samples μ inside the region $[\mu_{\min}, \mu_{\max}]^d$ and suggests the lowest Q -scoring μ that satisfy the condition $Q \leq \epsilon$ to constitute $S_{\mu'}$, which we call the *induced set*. The BBGAN treats the induced set as a training set, so the samples in $S_{\mu'}$ act as virtual samples from the fooling distribution $\mathbf{P}_{\mu'}$ that we want to learn. As the size of the induced set $|S_{\mu'}|$ increases, the BBGAN learns more of the distribution $\mathbf{P}_{\mu'}$. As $|S_{\mu'}| \rightarrow \infty$, any sample from $S_{\mu'}$ becomes a sample of $\mathbf{P}_{\mu'}$ and the BBGAN in Eq (6) satisfies the strict problem in Eq (3). Consequently, sampling from the adversary \mathbf{G} would consistently fool agent \mathbf{A} . We show this empirically in the **appendix**. The number of samples needed for $S_{\mu'}$ to be representative of $\mathbf{P}_{\mu'}$ depends on the search space which, in turn, depends on the dimensionality d of μ . Because of the black box and stochastic nature of \mathbf{E}_μ and \mathbf{A} (just like other RL environments) we follow the random sampling scheme common in RL [30] instead of the deterministic gradient estimation. In Section 5.3, we try different baseline methods to optimize the objective and summarize our findings in Table 1.

3.3. Special Cases of Adversarial Attacks

Pixel Adversarial Attack on Image Classifiers. Probably the most popular adversarial attack in the literature is a pixel-level perturbation to fool an image classifier. This attack can be thought of as a special case of our general formulation. In this case, the agent \mathbf{A} is a classifier \mathbf{C} and the environment \mathbf{E}_μ is a dataset containing the set Φ of all images in the classification dataset along with their respective

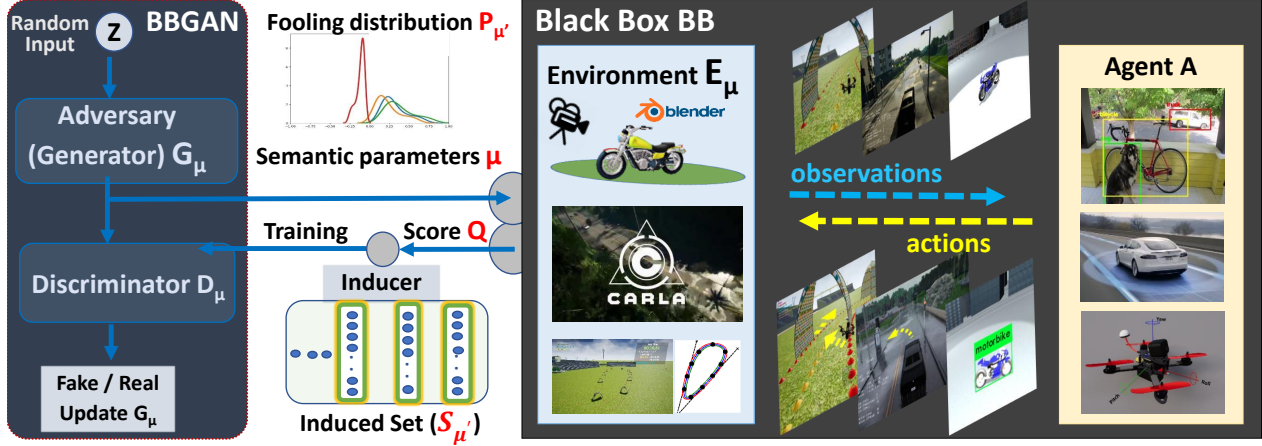


Figure 3: **BBGAN: Learning Fooling Distribution of Semantic Environment Parameters.** We learn adversary \mathbf{G} that can sample semantic parameters μ that parametrize the environment \mathbf{E}_μ , such that an agent \mathbf{A} would fail in a task in \mathbf{E}_μ . To achieve this an Inducer is used to induce a the induced set $S_{\mu'}$ that includes fooling parameter μ' and pass this as a training to the BBGAN. Three safety-critical applications are used to demonstrate this in three virtual environments: object detection, self-driving cars, and autonomous racing UAVs.

ground truth labels, *i.e.* $\{(\mathbf{x}_i, y_i)\}_{i=1}^{|\Phi|}$ and $y_i \in \{1, \dots, K\}$. Parameter μ defines the fooling noise to be added to the images (*i.e.* $d = n$). The observation is simply an image from Φ with noise added: $\mathbf{o}_t = \mathbf{x}_i + \mu$ for some $i \in \{1, 2, \dots, |\Phi|\}$. In classification, the environment is static with $T = 1$. The sole action \mathbf{a}_1 is simply the softmax score of the highest scoring class label predicted by \mathbf{C} that is not the true class y_i . Formally, $\mathbf{a}_1 = \max_{j \neq y_i} \mathbf{C}(\mathbf{x}_i + \mu) = l_j$. The reward function is $R(\mathbf{s}_1, \mathbf{a}_1) = \max(l_j - l_{y_i}, 0)$. Here, ϵ is the attack fooling threshold, whereby fooling occurs if $l_j - l_{y_i} \geq \epsilon$. For a single image attack, the hard constraint in Eq (3) becomes the constraint in Eq (1).

Semantic Adversarial Attack on Object Detectors. Extending adversarial attacks from classifiers to object detectors is straight-forward. We follow previous work [13] in defining the object detector as a function $\mathbf{F} : [0, 1]^n \rightarrow (\mathbb{R}^{N \times K}, \mathbb{R}^{N \times 4})$, which takes an n -dimensional image as input and outputs N detected objects. Each detected object has a probability distribution over K class labels and a 4-dimensional bounding box for the detected object. We take the top J proposals according to their confidence and discard the others. Analyzing the detector in our general setup is similar to the classifier case. The environment \mathbf{E}_μ is static (*i.e.* $T = 1$), and it contains all images with ground truth detections. For simplicity, we consider one object of interest per image (indexed by i). The observation in this case is a rendered image of an instance of object class i , where the environment parameter μ determines the 3D scene and how the image is rendered (*e.g.* the camera position/viewpoint, lighting directions, textures, *etc.*). Here, the observation is defined as the rendering function $\mathbf{o}_1 : [\mu_{\min}, \mu_{\max}]^d \rightarrow \mathbb{R}^n$. We use Blender [7] to render the 3D scene containing the object and to determine its ground truth bounding box location in the rendered image. The ac-

tion \mathbf{a}_1 by the agent/detector is simply the highest confidence score l_i corresponding to class i from the top J detected boxes in \mathbf{o}_1 . The final score of \mathbf{F} is $Q(\mathbf{F}, \mathbf{E}_\mu) = l_i$. The attack on \mathbf{F} is considered successful, if $l_i \leq \epsilon$.

Semantic Adversarial Attack on Autonomous Agents. The semantic adversarial attack of an autonomous agent can also be represented in the general formulation of Algorithm 1. Here, \mathbf{A} corresponds to the navigation policy, which interacts with a parametrized environment \mathbf{E}_μ . The environment parameter $\mu \in \mathbb{R}^d$ comprises d variables describing the weather/road conditions, camera pose, environment layout *etc.* In this case, an observation \mathbf{o}_t is an image as seen from the camera view of the agent at time t . The action \mathbf{a}_t produced by the navigation policy is the set of control commands (*e.g.* gas and steering for a car or throttle, pitch, roll and yaw for a UAV). The reward function $R(\mathbf{s}_t, \mathbf{a}_t)$ measures if the agent successfully completes its task (*e.g.* 1 if it safely reaches the target position at time t and 0 otherwise). The episode ends when either the agent completes its task or the maximum number of iterations T is exceeded.

4. Applications

4.1. Object Detection

Object detection is one of the essential perception tasks commonly used in autonomous navigation. In short, its goal is to determine the bounding box and class label of objects available in an image. You Only Look Once (YOLO) object detectors popularized a single-stage approach in which the detector observes the entire image and regresses the boundaries of the bounding boxes and the classes directly [39]. This approach trades off the accuracy of the detector for speed, making real-time object detection possible (passing the 30-FPS threshold).

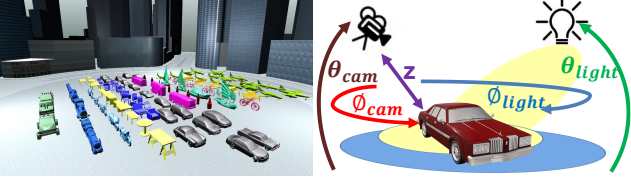


Figure 4: **Object Detection Attacks Setup:** *left:* the 100 shapes from Pascal3D [51] and ShapeNet [11] of 12 classes used in the YOLOV3 detection adversarial attacks. One shape from the intended class of attack is randomly picked and placed in the middle of a plaza in the Blender environment, rendered by the camera and then passed to the detector, YOLOV3. *Right:* the semantic parameters μ used: (z) : camera distance to the object, $(\phi_{cam}, \theta_{cam}, \phi_{light}, \theta_{light})$: camera azimuth, pitch and light source azimuth, and pitch angles respectively.

Agent. Based on its suitability for autonomous applications, we choose the very fast state-of-the-art YOLOv3 object detector as the agent [40]. It achieves a competitive mAP score on the MS-COCO detection benchmark and it can run in real-time [29].

Environment. We use Blender [7] to construct a scene based on freely available 3D scenes and CAD models from free3D [2] and 3Dwarehouse [1]. The scene was picked to be an urban scene with an open area to allow for different rendering setups. The scene includes one object of interest, one camera, and one main light source all directed toward the center of the object. The light is a fixed strength spotlight located at a fixed distance from the object. The material of each object is semi-metallic, which is common among the Pascal-3D object classes [51] we chose. Two classes (Sofa and TV-monitor) are not properly detected by YOLOv3, so they are replaced by two ShapeNet classes [11]. The 12 object classes are: aeroplane, bench, bicycle, boat, bottle, bus, car, chair, dining table, motorbike, train, and truck. The total number of shapes across all 12 classes is 100 as shown in Figure 2 (we augment Pascal3D shapes with others from Shapenet[11] and Modelnet40 [50]). One shape from the intended class is picked randomly for each iteration and placed in the middle of the Blender environment and the rendered image is passed to YOLOV3. The YOLO detector works adequately on these shapes with a Q score of at least 0.4 on each class. Please refer to the **appendix** for a more details regarding this dataset and our setup.

Input parameters. We take $\mu \in \mathbb{R}^8$, with parameters that have shown to affect detection performance and which frequently occur in real setups (refer to Figure 4). The object is centered in the virtual urban arena (diagnosis arena), and the camera circles around the object, while it is kept in the center of the rendered images. The parameters were normalized to $[\mu_{min}, \mu_{max}]^d = [-1, 1]^8$ before using them for learning and testing.

4.2. Self-Driving

There is a lot of recent work in autonomous driving especially in the fields of robotics and computer vision [8, 16, 37, 14]. In general, complete driving systems are very complex and difficult to analyze or simulate. By learning the underlying distribution of failure cases, our work provides a safe way to analyze the robustness of such a complete system. While our analysis is done in simulation only, we would like to highlight that sim-to-real transfer is a very active research field nowadays [38, 42, 43, 44, 48].

Agent. We use an autonomous driving agent (based on CIL [14]), which was trained on the environment E_μ with default parameters. The driving-policy was trained end-to-end to predict car controls given an input image and is conditioned on high-level commands such as *turn right at the next intersection* in order to facilitate autonomous navigation.

Environment. We use the recently released CARLA driving simulator [15], the most realistic open-source urban driving simulator currently available. We consider the three common tasks of going in a straight line, completing one turn, and navigating between two random points [15]. The score is measured as the average success of five pairs of start and end positions.

Input parameters. Since experiments are time consuming, we restrict ourselves to three parameters, two of which pertain to the mounted camera viewpoint and the third controls the appearance of the environment by changing the weather setting (e.g. 'clear noon', 'clear sunset', 'cloudy after rain', etc.). We describe these parameters in detail in the **appendix**. As such, we construct an environment by randomly perturbing the position and rotation of the default camera along the z -axis and around the pitch axis respectively, and by picking one of the weather conditions. Intuitively, this helps measure the robustness of the driving policy to the camera position (e.g. deploying the same policy in a different vehicle) and to environmental conditions.

4.3. UAV Racing

In recent years, UAV racing has emerged as a new sport where pilots compete in navigating small UAVs through race courses at neck-breaking speeds. Since this is a very interesting research problem, it has also been picked up by the robotics and vision communities [25, 35].

Agent. We use a fixed agent to autonomously fly through each course and measure its success as percentage of gates passed [35]. If the next gate was not reached within 10 seconds, we reset the agent at the last gate. We also record the time needed to complete the course. Our agent uses a perception network that produces waypoints and a PID controller to produce low-level controls.

Environment. We use the general-purpose simulator for computer vision applications, Sim4CV [33]. Sim4CV is not only versatile but also photo-realistic and provides a suit-

able environment for UAV racing.

Input parameters. In this application, we change the geometry of the environment. We define three different race track templates with 3, 4 and 5 2D anchor points, respectively. These points describe a second order B-spline and are perturbed to generate various race tracks delineated by colored cones and populated by uniformly spaced gates. Please refer to the **appendix** for more details and visualizations of the generated tracks.

5. Experiments

In our experimental setup, each method produces M samples (250 for object detection and 100 for self-driving and UAV racing) based on its model of the fooling distribution. We then compute the *attack fooling rate* (AFR) of the adversary. We use a fooling rate threshold of $\epsilon = 0.3$ [13], $\epsilon = 0.6$, and $\epsilon = 0.7$ for object detection, self-driving, and UAV racing, respectively. Next, we explain the experimental details of the baseline methods, our approach, and show quantitative results for each application with an analysis.

5.1. Baselines

Here, we describe all evaluated baseline methods for estimating the fooling distribution.

Random. We uniformly sample random parameters μ within the admissible range.

Gaussian Mixture Model (GMM). We fit a full covariance GMM of varying Gaussian components to estimate the distribution of the samples in the induced set $S_{\mu'}$. The baselines are denoted as Gaussian (one component), GMM10% and GMM50% (number of components as percentage of the samples in the induced set).

Bayesian Expected Improvement. We use the hyperopt [6] implementation of the Expected Improvement (EI) Bayesian Optimization algorithm [24] (adapted similarly by [49]). We perform the Bayesian optimization for 10K steps on the objective of the score Q for the detector. The optimizer will gradually sample more around the global minimum of the function. Hence, we use the last 1000 samples (induced set $S_{\mu'}$) that the optimizer sampled during the optimization and learn a GMM on that with different Gaussian components. Finally, we sample M parameter vectors from the GMMs and report results of the best model.

Multi-Class SVM. We bin the output score Q into 5 equally sized bins and train a multi-class SVM classifier on the complete dataset to predict the correct bin. We then randomly sample parameter vectors μ , classify them, and sort them by the predicted score. We then pick the top M number of samples with the lowest score Q .

Gaussian Process Regression. We train a Gaussian Process Regressor with exponential kernel to regress the scores. We then randomly sample vectors μ , regress them to their score Q , sort them, and pick the top M samples.

5.2. BBGAN

Here, we show how our proposed BBGAN can be used to estimate the distribution of failure cases with respect to some environment parameters μ that affect the observations from the environment in which the agent operates.

Training. To learn the fooling distribution $P_{\mu'}$ in Section 3.1, we train the BBGAN as described in Section 3.2. We use a vanilla GAN [18], but any GAN architecture can be used. We use a simple FCN with 2 layers for the Generator G and Discriminator D . We train the GAN following convention, but since we do not have access to the true distribution that we want to learn (*i.e.* real samples), we *induce* the set by randomly sampling N parameter vector samples μ , and then picking the K worst performing ones among them. For object detection, $N = 20K$ image renderings for each class (a total of 240K images), as described in Section 3.3. For autonomous driving, $N = 1000$ samples for each driving task as described in Section 4.2. For UAV racing, $N = 1000$ tracks are randomly generated as described in Section 4.3.

Testing. We sample M parameters μ from the learnt BBGAN, and then evaluate the agent in the M corresponding environments to obtain the score $Q(\mu)$ for each sample. We then compute the average fooling rate according to the fooling threshold ϵ .

5.3. Results

Table 1 summarizes the results of the fooling rate for several baselines and our approach across all three applications. For object detection, we show 3 out of 12 classes and report the average across all classes. For autonomous driving, we report the results on all three tasks as described in Section 4.2. For UAV racing, we report the results for three different track types, parameterized by 3, 4 and 5 anchor points (refer to Section 4.3).

Our results show that we consistently outperform the baselines, even the ones that were trained on the complete dataset rather than the smaller induced set, such as the multi-class SVM and the GP regressor. While most baselines perform well on the autonomous driving application where μ consists of only 3 parameters, our approach performs especially well on higher dimensional environments. For object detection (8 parameters) and UAV racing (10 parameters), we outperform all baselines by a large margin. To ensure that mode collapse (a GAN phenomenon where the generator collapses to generate a single point because of imbalance loss with the discriminator) did not occur, we do the following: we visualize the generated parameters and we measure their μ_{std} , the mean of the standard deviation per parameter dimension to make sure it is not zero.

5.4. Analysis

The usefulness of SADA lies in that it is not only an attacking scheme, but it also can serve as a diagnosis tool to

| | Object Detection | | | | Autonomous Driving | | | UAV Track Generation | | |
|-----------------|------------------|-----------|-------|--------------|--------------------|-----------|------------|----------------------|-----------|-----------|
| | Bicycle | Motorbike | Truck | 12-class avg | Straight | One Curve | Navigation | 3 anchors | 4 anchors | 5 anchors |
| Full Set | 14.6% | 32.5% | 56.8% | 37.1 % | 10.6% | 19.5% | 46.3% | 17.0% | 23.5% | 15.8% |
| Random | 13.3% | 38.8% | 73.8% | 45.7% | 8.0% | 18.0% | 48.0% | 22.0% | 30.0% | 16.0% |
| Multi-Class SVM | 20.0% | 45.6% | 70.8% | 45.8% | 96.0% | 100% | 100% | 24.0% | 30.0% | 14.0% |
| GP Regression | 17.6% | 43.6% | 83.6% | 45.26% | 100% | 100% | 100% | 74.0% | 94.0% | 44.0% |
| Gaussian | 19.6% | 40.4% | 72.4% | 47.0% | 54.0% | 30.0% | 64.0% | 49.3% | 56.0% | 28.7% |
| GMM10% | 26.0% | 48.4% | 75.2% | 49.0% | 90.0% | 72.0% | 98.0% | 57.0% | 63.0% | 33.0% |
| GMM50% | 16.4% | 46.8% | 72.0% | 47.8% | 92.0% | 68.0% | 100% | 54.0% | 60.0% | 40.0% |
| Bayesian [49] | 48.0% | 52.0% | 75.6% | 56.1% | - | - | - | - | - | - |
| BBGAN (ours) | 44.0% | 45.2% | 90.8% | 74.5% | 100% | 56.0% | 98.0% | 42.0% | 52.0% | 86.0% |
| BBGAN (boost) | 65.8% | 82.0% | 100% | 80.5% | 100% | 84.0% | 100% | 86.0% | 58.0% | 92.0% |

Table 1: **Attack Fooling Rate Comparison:** AFR of adversarial attack on three safety-critical applications: YOLOV3 object detection, self-driving, and UAV racing. The threshold of fooling is 0.3, 0.6, 0.7 for the the above three applications respectively. In the YOLO experiment, we sample 250 parameter sets from each baseline and our model. We sample a shape from the intended class, render it according to the sampled parameters and detect by YOLOV3 to obtain the confidence score Q . Lastly, we calculate the AFR over all 250 points and show the performance for 3 out of the 12 classes and the average performance over all the 12 classes. For autonomous driving (CARLA) and UAV racing (Sim4CV), we sample 50 parameters and compute the AFR. We see that our BBGAN outperform all the baselines in most of the tasks, especially for high dimensional tasks like the detection experiment with YOLOV3 (8 parameters) and UAV racing (up to 12 parameters). Adding the boosting strategy to BBGAN can help to improve the AFR further. Due to the expensive computations of sequential nature of the Bayesian baseline, we omit it for the two autonomous navigation applications. More details are provided in Section 5, and Section 4.

assess the systemic failures of agents under certain setups that can occur in real-life scenarios.

To demonstrate the diagnostic merit of SADA, we restrict some of the parameters in Section 4.1, and study the four parameters (ϕ_{cam} , θ_{cam} , ϕ_{light} , θ_{light}) using SADA on two classes of interest: cars and motorbikes. We use BBGAN as our distribution learning method and we use the same setup as in Section 5.

To demonstrate the transferability of this attacking distribution to real-life, we photograph a toy motorbike, similar to the 3D model we are attacking, using a mobile camera and an office spotlight to replace the light source in the virtual environment. We take photos under different camera views and lighting directions (uniform sampling). We also take photos based on samples from the distribution learned by the BBGAN. We apply the YOLOv3 detector on these images and observe the confidence score for the ‘motorbike’ class of interest. On the samples generated from the BBGAN distribution, the fooling rate of attack is 21% as compared to only 4.3% if a random other viewpoint was taken. To show the transferability of the attacks to different shapes, we learn BBGAN on two detailed motorbike CAD models (not in our dataset) and then generate parameters and test on our motorbike class from the dataset with random picking during test time. We achieve AFR of 94.0% and 84.4% respectively compared to the random baselines of 48.0% and 43.2% respectively. This successful attack was conducted by learning fooling distribution on a single detailed CAD model and transferring the attack to the dataset. More details and more examples of similar diagnosis cases are presented in the **appendix**.

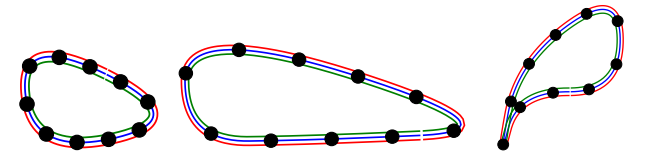


Figure 5: **Qualitative Examples:** *top*: generated samples from our BBGAN that fool YOLOV3 detector on two classes: truck, and motorbikes. *bottom*: generated tracks that fool UAV navigation system generated from BBGAN. All the samples generated are fooling adversarial attacks, with diverse samples per model.

6. Conclusion and Future Work

In the future we plan to investigate defense mechanisms for semantic attacks as described in this work. Specifically our method can be used to identify difficult samples that lie in the fooling distribution. These samples can then be used to train more robust classifiers for object detection and more robust agents for autonomous navigation policies.

References

- [1] 3d warehouse. <https://3dwarehouse.sketchup.com/?hl=en>, 2018.
- [2] Free3d. <https://free3d.com/>, 2018.
- [3] M. Arjovsky, S. Chintala, and L. Bottou. Wasserstein gan, 2017. arXiv:1701.07875.
- [4] A. Athalye, L. Engstrom, A. Ilyas, and K. Kwok. Synthesizing robust adversarial examples. *CoRR*, abs/1707.07397, 2017.
- [5] C. Audet and W. Hare. *Derivative-Free and Blackbox Optimization, chapter:3*, pages 33–54. Springer International Publishing, Cham, 2017.
- [6] J. Bergstra, B. Komer, C. Eliasmith, D. Yamins, and D. Cox. Hyperopt: A python library for model selection and hyperparameter optimization. *Computational Science & Discovery*, 8:014008, 07 2015.
- [7] Blender Online Community. *Blender - a 3D modelling and rendering package*. Blender Foundation, Blender Institute, Amsterdam, 2018.
- [8] M. Bojarski, D. D. Testa, D. Dworakowski, B. Firner, B. Flepp, P. Goyal, L. D. Jackel, et al. End to end learning for self-driving cars. *arXiv:1604.07316*, 2016.
- [9] N. Carlini and D. Wagner. Towards evaluating the robustness of neural networks. In *IEEE Symposium on Security and Privacy (SP)*, 2017.
- [10] N. Carlini and D. A. Wagner. Audio adversarial examples: Targeted attacks on speech-to-text. *CoRR*, abs/1801.01944, 2018.
- [11] A. X. Chang, T. Funkhouser, L. Guibas, P. Hanrahan, Q. Huang, Z. Li, S. Savarese, M. Savva, S. Song, H. Su, J. Xiao, L. Yi, and F. Yu. ShapeNet: An Information-Rich 3D Model Repository. Technical Report arXiv:1512.03012 [cs.GR], Stanford University — Princeton University — Toyota Technological Institute at Chicago, 2015.
- [12] P.-Y. Chen, H. Zhang, Y. Sharma, J. Yi, and C.-J. Hsieh. Zoo: Zeroth order optimization based black-box attacks to deep neural networks without training substitute models. In *Proceedings of the 10th ACM Workshop on Artificial Intelligence and Security, AISec '17*, pages 15–26, New York, NY, USA, 2017. ACM.
- [13] S. Chen, C. Cornelius, J. Martin, and D. H. Chau. Robust physical adversarial attack on faster R-CNN object detector. *CoRR*, abs/1804.05810, 2018.
- [14] F. Codevilla, M. Müller, A. Dosovitskiy, A. López, and V. Koltun. End-to-end driving via conditional imitation learning. In *ICRA*, 2018.
- [15] A. Dosovitskiy, G. Ros, F. Codevilla, A. López, and V. Koltun. CARLA: An open urban driving simulator. In *CoRL*, 2017.
- [16] U. Franke. Autonomous driving. In *Computer Vision in Vehicle Technology*. 2017.
- [17] Y. Freund and R. E. Schapire. A decision-theoretic generalization of on-line learning and an application to boosting. *J. Comput. Syst. Sci.*, 55(1):119–139, Aug. 1997.
- [18] I. Goodfellow, J. Pouget-Abadie, M. Mirza, B. Xu, D. Warde-Farley, S. Ozair, A. Courville, and Y. Bengio. Generative adversarial nets. In Z. Ghahramani, M. Welling, C. Cortes, N. D. Lawrence, and K. Q. Weinberger, editors, *Advances in Neural Information Processing Systems 27*, pages 2672–2680. Curran Associates, Inc., 2014.
- [19] I. Goodfellow, J. Shlens, and C. Szegedy. Explaining and harnessing adversarial examples. In *International Conference on Learning Representations*, 2015.
- [20] S. Gurumurthy, R. Kiran Sarvadevabhatla, and R. Venkatesh Babu. Deligan : Generative adversarial networks for diverse and limited data. In *The IEEE Conference on Computer Vision and Pattern Recognition (CVPR)*, July 2017.
- [21] H. Hosseini and R. Poovendran. Semantic adversarial examples. *CoRR*, abs/1804.00499, 2018.
- [22] P. Isola, J.-Y. Zhu, T. Zhou, and A. A. Efros. Image-to-image translation with conditional adversarial networks. *arxiv*, 2016.
- [23] J. Johnson, A. Alahi, and F. fei Li. Perceptual losses for real-time style transfer and super-resolution. In *ECCV*, 2016.
- [24] D. R. Jones, M. Schonlau, and W. J. Welch. Efficient global optimization of expensive black-box functions. *J. of Global Optimization*, 13(4):455–492, Dec. 1998.
- [25] E. Kaufmann, A. Loquercio, R. Ranftl, A. Dosovitskiy, V. Koltun, and D. Scaramuzza. Deep drone racing: Learning agile flight in dynamic environments. In A. Billard, A. Dragan, J. Peters, and J. Morimoto, editors, *Proceedings of The 2nd Conference on Robot Learning*, volume 87 of *Proceedings of Machine Learning Research*, pages 133–145. PMLR, 29–31 Oct 2018.
- [26] A. Kurakin, I. J. Goodfellow, and S. Bengio. Adversarial examples in the physical world. *CoRR*, abs/1607.02533, 2016.
- [27] A. Kurakin, I. J. Goodfellow, and S. Bengio. Adversarial machine learning at scale. *CoRR*, abs/1611.01236, 2016.
- [28] C. Ledig, L. Theis, F. Huszar, J. Caballero, A. Cunningham, A. Acosta, A. Aitken, A. Tejani, J. Totz, Z. Wang, and W. Shi. Photo-realistic single image super-resolution using a generative adversarial network. In *The IEEE Conference on Computer Vision and Pattern Recognition (CVPR)*, July 2017.
- [29] T.-Y. Lin, M. Maire, S. Belongie, J. Hays, P. Perona, D. Ramanan, P. Dollr, and C. L. Zitnick. Microsoft coco: Common objects in context. In *European Conference on Computer Vision (ECCV)*, Zrich, 2014. Oral.
- [30] H. Mania, A. Guy, and B. Recht. Simple random search provides a competitive approach to reinforcement learning. *CoRR*, abs/1803.07055, 2018.
- [31] S.-M. Moosavi-Dezfooli, A. Fawzi, O. Fawzi, and P. Frossard. Universal adversarial perturbations. In *The IEEE Conference on Computer Vision and Pattern Recognition (CVPR)*, July 2017.
- [32] S.-M. Moosavi-Dezfooli, A. Fawzi, and P. Frossard. Deepfool: A simple and accurate method to fool deep neural networks. In *The IEEE Conference on Computer Vision and Pattern Recognition (CVPR)*, June 2016.
- [33] M. Müller, V. Casser, J. Lahoud, N. Smith, and B. Ghanem. Sim4cv: A photo-realistic simulator for computer vision applications. *Int. J. Comput. Vision*, 126(9):902–919, Sept. 2018.
- [34] M. Müller, V. Casser, N. Smith, D. L. Michels, and B. Ghanem. Teaching UAVs to Race Using Sim4CV. *ArXiv e-prints*, Aug. 2017.

- [35] M. Müller, V. Casser, N. Smith, D. L. Michels, and B. Ghanem. Teaching UAVs to Race: End-to-End Regression of Agile Controls in Simulation. In *European Conference on Computer Vision Workshop (ECCVW)*, Sept. 2018.
- [36] A. Nitin Bhagoji, W. He, B. Li, and D. Song. Practical black-box attacks on deep neural networks using efficient query mechanisms. In *The European Conference on Computer Vision (ECCV)*, September 2018.
- [37] B. Paden, M. Cáp, S. Z. Yong, D. S. Yershov, and E. Frazzoli. A survey of motion planning and control techniques for self-driving urban vehicles. *IEEE Transactions on Intelligent Vehicles*, 1(1), 2016.
- [38] X. Pan, Y. You, Z. Wang, and C. Lu. Virtual to real reinforcement learning for autonomous driving. In *BMVC*, 2017.
- [39] J. Redmon, S. Divvala, R. Girshick, and A. Farhadi. You only look once: Unified, real-time object detection. In *The IEEE Conference on Computer Vision and Pattern Recognition (CVPR)*, June 2016.
- [40] J. Redmon and A. Farhadi. Yolov3: An incremental improvement. *CoRR*, abs/1804.02767, 2018.
- [41] S. Ren, K. He, R. Girshick, and J. Sun. Faster r-cnn: Towards real-time object detection with region proposal networks. In C. Cortes, N. D. Lawrence, D. D. Lee, M. Sugiyama, and R. Garnett, editors, *Advances in Neural Information Processing Systems 28*, pages 91–99. Curran Associates, Inc., 2015.
- [42] A. A. Rusu, M. Vecerik, T. Rothörl, N. Heess, R. Pascanu, and R. Hadsell. Sim-to-real robot learning from pixels with progressive nets. In *CoRL*, 2017.
- [43] F. Sadeghi and S. Levine. CAD2RL: Real single-image flight without a single real image. In *RSS*, 2017.
- [44] F. Sadeghi, A. Toshev, E. Jang, and S. Levine. Sim2Real view invariant visual servoing by recurrent control. *CVPR*, 2018.
- [45] M. Sharif, S. Bhagavatula, L. Bauer, and M. K. Reiter. Accessorize to a crime: Real and stealthy attacks on state-of-the-art face recognition. In *Proceedings of the 2016 ACM SIGSAC Conference on Computer and Communications Security, CCS '16*, pages 1528–1540, New York, NY, USA, 2016. ACM.
- [46] R. S. Sutton and A. G. Barto. *Introduction to Reinforcement Learning*. MIT Press, Cambridge, MA, USA, 1st edition, 1998.
- [47] C. Szegedy, W. Zaremba, I. Sutskever, J. Bruna, D. Erhan, I. J. Goodfellow, and R. Fergus. Intriguing properties of neural networks. *CoRR*, abs/1312.6199, 2013.
- [48] J. Tobin, R. Fong, A. Ray, J. Schneider, W. Zaremba, and P. Abbeel. Domain randomization for transferring deep neural networks from simulation to the real world. In *IROS*, 2017.
- [49] V. Veeravasarapu, C. Rothkopf, and R. Visvanathan. Adversarially tuned scene generation. In *The IEEE Conference on Computer Vision and Pattern Recognition (CVPR)*, July 2017.
- [50] Z. Wu, S. Song, A. Khosla, F. Yu, L. Zhang, X. Tang, and J. Xiao. 3d shapenets: A deep representation for volumetric shapes. In *2015 IEEE Conference on Computer Vision and Pattern Recognition (CVPR)*, pages 1912–1920, June 2015.
- [51] Y. Xiang, R. Mottaghi, and S. Savarese. Beyond pascal: A benchmark for 3d object detection in the wild. In *IEEE Winter Conference on Applications of Computer Vision (WACV)*, 2014.
- [52] C. Xie, J. Wang, Z. Zhang, Y. Zhou, L. Xie, and A. Yuille. Adversarial examples for semantic segmentation and object detection. In *The IEEE International Conference on Computer Vision (ICCV)*, Oct 2017.
- [53] S. Xie, Z. Chen, C. Xu, and C. Lu. Environment upgrade reinforcement learning for non-differentiable multi-stage pipelines. In *The IEEE Conference on Computer Vision and Pattern Recognition (CVPR)*, June 2018.
- [54] R. Yeh, C. Chen, T. Lim, M. Hasegawa-Johnson, and M. N. Do. Semantic image inpainting with perceptual and contextual losses. *CoRR*, abs/1607.07539, 2016.
- [55] X. Zeng, C. Liu, Y. Wang, W. Qiu, L. Xie, Y. Tai, C. Tang, and A. L. Yuille. Adversarial attacks beyond the image space. *CoRR*, abs/1711.07183, 2017.

A. Empirical Justification for BBGAN

As the size of the induced set $|S_{\mu'}| \rightarrow \infty$, the following objective of the black box GAN (BBGAN) holds:

$$\min_{\mathbf{G}_\mu} \max_{\mathbf{D}_\mu} L_{\text{BBGAN}}(\mathbf{G}_\mu, \mathbf{D}_\mu, S_{\mu'}) = \mathbb{E}_{\mu \sim S_{\mu'}} [\log \mathbf{D}_\mu(\mu)] + \mathbb{E}_{\mathbf{z} \sim p_{\mathbf{z}}(\mathbf{z})} [\log(1 - \mathbf{D}(\mathbf{G}(\mathbf{z})))] \quad (7)$$

By solving this objective we learn an adversary \mathbf{G}_μ that converges when it has the same distribution as the fooling distribution of semantic parameters $\mathbf{P}_{\mu'}$ defined as follows:

$$\mu' \sim \mathbf{P}_{\mu'} \Leftrightarrow Q(\mathbf{A}, \mathbf{E}_{\mu'}) \leq \epsilon; \quad \mu' \in [\mu_{\min}, \mu_{\max}]^d \quad (8)$$

Here, the agent \mathbf{A} lives in the environment \mathbf{E}_μ that gives a score Q according to a threshold ϵ for a given parameter μ .

Empirical Proof.

We use the definition of Exhaustive Search (Algorithm 3.1) from the Audet and Hare book on derivative-free and black box optimization [5]. With this definition in mind, we try to optimize an objective $f : \mathbb{R}^d \rightarrow \mathbb{R}$ defined on a closed continuous global set Ω by densely sampling a countable subset $S = \{\mu_1, \mu_2, \dots, \mu_N\} \subset \Omega$. Theorem 3.1 [5] states that as long as the exhaustive search continues to infinity from the set S (i.e. as $N \rightarrow \infty$) the global solutions μ^* can be obtained by the following optimization:

$$\mu^* = \arg \min_{\mu} f(\mu) \quad \text{s.t. } \mu \in \Omega \quad (9)$$

where the best solution μ_N^{best} is reached up to the sample μ_N . If the set S_{μ^*} is the set of all global solutions μ^* , then

$$\mu_N^{\text{best}} \in S_{\mu^*} = \{\mu^*\}, \quad \text{as } N \rightarrow \infty \quad (10)$$

Now let $f(\mu) = \max(0, Q(\mathbf{E}_\mu, \mathbf{A}) - \epsilon)$ and let $\Omega = [\mu_{\min}, \mu_{\max}]$, then the global solutions of the optimization:

$$\begin{aligned} \mu^* &= \arg \min_{\mu} \max(0, Q(\mathbf{E}_\mu, \mathbf{A}) - \epsilon) \\ \text{s.t. } \mu &\in [\mu_{\min}, \mu_{\max}] \end{aligned} \quad (11)$$

satisfy the two conditions in Eq (8).

$$Q(\mathbf{A}, \mathbf{E}_{\mu^*}) \leq \epsilon; \quad \mu^* \in [\mu_{\min}, \mu_{\max}]^d \quad (12)$$

Hence, the set of all global solutions includes all the points in the fooling distribution:

$$S_{\mu^*} = \{\mu^*\} = \{\mu' : \mu' \sim \mathbf{P}_{\mu'}\} \quad (13)$$

Hence, as the sampling set size $|S| \rightarrow \infty$, all the points μ that lead to $Q(\mathbf{E}_\mu, \mathbf{A}) \leq \epsilon$, achieve the minimum objective in Eq (11) of zero and hence the set of best observed

values $|\{\mu_N^{\text{best}}\}| \rightarrow \infty$. This set is what we call the induced set $S_{\mu'}$ and from Eq (10), we can infer the following:

$$\text{as } N \rightarrow \infty, \quad S_{\mu'} \rightarrow \{\mu' : \mu' \sim \mathbf{P}_{\mu'}\} \quad (14)$$

Finally if the set $S_{\mu'}$ has converged to the distribution $\mathbf{P}_{\mu'}$ and we use $S_{\mu'}$ to train the BBGAN in Eq (7), then according to proposition 2 from the original GAN paper by Goodfellow *et al.* [18], the adversary \mathbf{G}_μ has learnt the distribution $\mathbf{P}_{\mu'}$ and hence satisfies the following equation:

$$\begin{aligned} \arg \min_{\mathbf{G}_\mu} \mathbb{E}_{\mu \sim \mathbf{G}} [Q(\mathbf{A}, \mathbf{E}_\mu)] \\ \text{s.t. } \{\mu : \mu \sim \mathbf{G}_\mu\} = \{\mu' : \mu' \sim \mathbf{P}_{\mu'}\} \end{aligned} \quad (15)$$

This concludes our empirical proof for our BBGAN.

B. Boosting Strategy for BBGAN

B.1. Intuition for Boosting

Inspired by the classical Adaboost meta-algorithm [17], we use a boosting strategy to improve the performance of our BBGAN trained in Section 5 of our paper with results reported in Table 1. The boosting strategy of BBGAN is simply utilizing the information learned from one BBGAN by another BBGAN in a sequential manner. The intuition is that the main computational burden in training the BBGAN is not the GAN training but computing the agent \mathbf{A} episodes (which can take multiple hours per episode in the case of the self-driving experiments).

B.2. Description of Boosting for BBGANs

We propose to utilize the generator to generate samples that can be used by the next BBGAN. We start by creating the set Ω_0 of the first stage adversary \mathbf{G}_0 . We then simply add the generated parameters μ along with their computed scores Q to the training data of the next stage BBGAN (i.e. BBGAN-1). We start the next stage by inducing a new induced set $S_{\mu'}^1$, (that may include part or all the previous stage induced set $S_{\mu'}^0$). However, the aim is to put more emphasis on samples that were generated in the previous stage. Hence, the inducer in the next stage can just randomly sample N points, compute their Q scores and add $\beta * N$ generated samples from BBGAN-0 to the N random samples. The entire set is then sorted based on the Q scores and the lowest-scoring M points that satisfy Eq (8) are picked as the induced set $S_{\mu'}^1$. The BBGAN-1 is then trained according to Eq (7). Here β is the boosting rate of our boosting strategy which dictates how much emphasis is put on the previous stage (exploitation ratio) when training the next stage. The whole boosting strategy can be repeated more than once. Algorithm 2 summarizes the boosting meta-algorithm for BBGAN. The global set Ω of all N sampled points and the update rule from one stage to another is described by the following two equations:

Algorithm 2: Boosting Strategy for BBGAN

Requires: environment E_μ , Agent **A** number of boosting stages K , boosting rate β , initial training size N
Sample N points to form Ω_0 like in Eq (16)
induce $S_{\mu'}^0$ from Ω_0
learn adversary \mathbf{G}_0 according to Eq (7)
for $i \leftarrow 1$ **to** K **do**
 update boosted training set Ω_i from Ω_{i-1} as in Eq (17)
 obtain $S_{\mu'}^i$ from Ω_i
 train adversary \mathbf{G}_i as in Eq (7)
end
Returns: last adversary \mathbf{G}_K

$$\Omega_0 = \{\mu_j \sim \text{Uniform}(\mu_{\min}, \mu_{\max})\}_{j=1}^N \quad (16)$$

$$\Omega_{k+1} = \Omega_k \cup \{\mu_j \sim \mathbf{G}_k\}_{j=1}^{\lfloor \beta N \rfloor} \quad (17)$$

These global sets Ω_k constitute the basis from which the inducer produces the induced sets $S_{\mu'}^k$. The adversary \mathbf{G}_k of boosting stage k uses this induced set when training according to the BBGAN objective in Eq (7).

B.3. Experimental Details for Boosting

We note that low β values do not affect the training of our BBGAN since the induced set will generally be the same. Hence, we use $\beta = 0.5$, a high boosting rate. For practical reasons (computing 50% of the training data per boosting stage is expensive) we just compute 10% of the generated data and repeat it 5 times. This helps to stabilize the BBGAN training and forces it to focus more on samples that have low scores without having to evaluate the score function on 50% of the training data.

C. Detailed Results

Tables 2 and 3 show the detailed results for all three applications.

D. Analysis - Diagnosis and Transferability

We provide an analysis for the task of object detection in what follows. The goal is to provide some diagnosis of failure cases and explore transferability to the real-world. We investigate transfer to more complex and detailed shapes of the same class. For these experiments we restrict ourselves to setups common in the real-world and restrict the number of parameters.

View point. We restrict the number of parameters to 4 parameters ($\phi_{\text{cam}}, \theta_{\text{cam}}, \phi_{\text{light}}, \theta_{\text{light}}$), and fix the object class and RGB colors (pure blue). We use two classes (car and motorbike) in order to investigate the effect of the shape within a class. To this end we use detailed shapes with textures of the general class used in the main experiment in the

paper. The total number of scenarios is 5: generic car (scenario 1), generic motorbike (scenario 2), detailed car model (scenario 3), detailed motorbike 1 (scenario 4) and detailed motorbike 2 (scenario 5). Figures 7, 8, 9, 10 and 11 show qualitative results for each scenario.

Occlusion. Since occlusion plays an important role in object mis-detection, we introduce an occlusion experiment. Here, we investigate how occlusion (*e.g.* by a pole) can result in failure of a detector (*e.g.* from which view point). Therefore, we included the camera viewpoint angles ($\phi_{\text{cam}}, \theta_{\text{cam}}$) and introduce a third parameter to control horizontal shift of a pole that covers 15% of the rendered image and moves from one end to another. The pole keeps a fixed distance to the camera and is placed between the camera and the object. Like in the previous study, the total number of scenarios is 5: generic car (scenario 6), generic motorbike (scenario 7), detailed car model (scenario 8), detailed motorbike 1 (scenario 9), and detailed motorbike 2 (scenario 10). Figures 12, 13, 14, 15 and 16 show qualitative results for each scenario.

Visualization. In Figures 17 and 18, we visualize of the fooling distribution generated by our BBGAN in the two previous experiments (Section D). We also include some real-world images captured according to the parameters generated by the BBGAN.

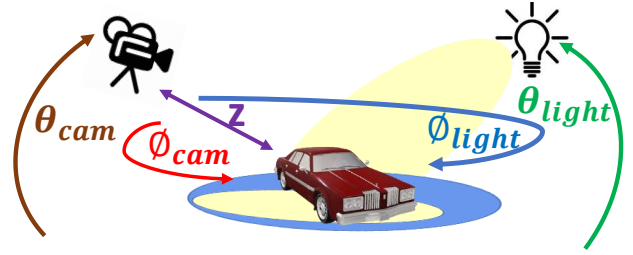


Figure 6: **Visualization view point parameters** These parameters are used in the first analysis experiment. The object class and RGB colors are fixed.

E. Qualitative Examples

Figure 19 shows some qualitative examples for each of the 12 object classes. These images were rendered according to parameters generated by BBGAN which fooled the detector.

F. Insights Gained by BBGAN Experiments

F.1. Object Detection with YOLOV3:

In our YOLOV3 experiments, we consistently found that for most objects top rear or top front views of the object are fooling the YOLOV3 detector. Furthermore, the light angle which will result in highest reflection off the surface of the object also results in higher fooling rates for the detector.

| | aeroplane | bench | bicycle | boat | bottle | bus | car | chair | diningtable | motorbike | train | truck | avg | μ_{std} |
|-----------------|-----------|-------|---------|-------|--------|-------|-------|-------|-------------|-----------|-------|-------|--------|-------------|
| Full Set | 8.64% | 35.2% | 14.6% | 33.4% | 22.5% | 53.1% | 39.8% | 44.1% | 46.1% | 32.5% | 58.1% | 56.8% | 37.1 % | 0.577 |
| Random: | 11.3% | 42.7% | 18.6% | 41.8% | 28.4% | 65.7% | 49.9% | 55.3% | 56.4% | 40.3% | 72.8% | 70.8% | 46.2% | 0.584 |
| Multi-Class SVM | 12.0% | 45.6% | 20.0% | 39.6% | 26.0% | 64.4% | 49.6% | 50.4% | 53.6% | 45.6% | 72.0% | 70.8% | 45.8% | 0.576 |
| GP Regression | 13.6% | 15.6% | 17.6% | 41.2% | 31.6% | 71.6% | 51.6% | 48.0% | 56.0% | 43.6% | 69.2% | 83.6% | 45.26% | 0.492 |
| Gaussian | 11.2% | 45.6% | 19.6% | 41.6% | 31.2% | 70.4% | 48.0% | 56.8% | 55.6% | 40.4% | 71.2% | 72.4% | 47.0% | 0.548 |
| GMM10% | 14.8% | 45.2% | 26.0% | 42.8% | 34.0% | 67.2% | 53.2% | 56.4% | 54.8% | 48.4% | 70.4% | 75.2% | 49.0% | 0.567 |
| GMM50% | 12.0% | 44.0% | 16.4% | 46.4% | 33.2% | 66.4% | 51.6% | 53.2% | 58.4% | 46.8% | 73.6% | 72% | 47.8% | 0.573 |
| Bayesian [49] | 9.2% | 42.0% | 48.0% | 68.8% | 32.4% | 91.6% | 42.0% | 75.6% | 58.4% | 52.0% | 77.2% | 75.6% | 56.1% | 0.540 |
| BBGAN (ours) | 13.2% | 91.6% | 44.0% | 90.0% | 54.4% | 91.6% | 81.6% | 93.2% | 99.2% | 45.2% | 99.2% | 90.8% | 74.5% | 0.119 |
| BBGAN (boost) | 33% | 82.4% | 65.8% | 78.8% | 67.4% | 100% | 67.4% | 100% | 90.2% | 82.0% | 98.4% | 100% | 80.5% | 0.100 |

Table 2: Fooling rate of adversarial attacks on different classes of the augmented Pascal3D dataset. We sample 250 parameters after the training phase of each model and sample a shape from the intended class. We then render an image according to these parameters and run the YOLOV3 detector to obtain a confidence score of the intended class. If this score $Q \leq \epsilon = 0.3$, then we consider the attack successful. The fooling rate is then recorded for that model, while μ_{std} (the mean of standard deviations of each parameter dimensions) is recorded for each model. We report the average over all classes. This metric represents how varied the samples from the attacking distribution are.

| | Straight | | One Curve | | Navigation | | 3 control points | | 4 control points | | 5 control points | |
|-----------------|----------|-------------|-----------|-------------|------------|-------------|------------------|-------------|------------------|-------------|------------------|-------------|
| | FR | μ_{std} | FR | μ_{std} | FR | μ_{std} | FR | μ_{std} | FR | μ_{std} | FR | μ_{std} |
| Full Set | 10.6% | 0.198 | 19.5% | 0.596 | 46.3% | 0.604 | 17.0% | 0.607 | 23.5% | 0.544 | 15.8% | 0.578 |
| Random | 8.0% | 0.194 | 18.0% | 0.623 | 48.0% | 0.572 | 22.0% | 0.602 | 30.0% | 0.550 | 16.0% | 0.552 |
| Multi-Class SVM | 96.0% | 0.089 | 100% | 0.311 | 100% | 0.517 | 24.0% | 0.595 | 30.0% | 0.510 | 14.0% | 0.980 |
| GP Regression | 100% | 0.014 | 100% | 0.268 | 100% | 0.700 | 74.0% | 0.486 | 94.0% | 0.492 | 44.0% | 0.486 |
| Gaussian | 54.0% | 0.087 | 30.0% | 0.528 | 64.0% | 0.439 | 49.3% | 0.573 | 56.0% | 0.448 | 28.7% | 0.568 |
| GMM10% | 90.0% | 0.131 | 72.0% | 0.541 | 98.0% | 0.571 | 57.0% | 0.589 | 63.0% | 0.460 | 33.0% | 0.558 |
| GMM50% | 92.0% | 0.122 | 68.0% | 0.556 | 100% | 0.559 | 54.0% | 0.571 | 60.0% | 0.478 | 40.0% | 0.543 |
| BBGAN (ours) | 100% | 0.048 | 56.0% | 0.526 | 98.0% | 0.137 | 42.0% | 0.161 | 52.0% | 0.214 | 86.0% | 0.202 |
| BBGAN (boost) | 100% | 0.014 | 84.0% | 0.103 | 100% | 0.058 | 86.0% | 0.084 | 58.0% | 0.219 | 92.0% | 0.003 |

Table 3: Autonomous Driving (CARLA) and UAV Racing Track Generation (Sim4CV). Each method produces 50 samples and we show the fooling rate (FR) and the mean of the standard deviation per parameter. We set the fooling threshold to 0.6 and 0.7 for autonomous driving and racing track generation respectively.

The color of the object does not play a big role in fooling the detector, but usually colors that are closer to the background color tend to be preferred by the BBGAN samples (as shown in the qualitative examples). From the analysis in Section D of transferability of these attacks, we note that attacks on more detailed CAD shapes and models transfer better to less detailed shapes, but the opposite is not true.

F.2. Self-driving cars:

In our experiments we found that weather is the least important parameter for determining success. This is probably due to the fact that the driving policy was trained on multiple weather conditions. This allows for some generalization and robustness to changing weather conditions. However, the driving policy was trained with a fixed camera. We observe, that the driving policy is very sensitive to slight perturbations of the camera pose (height and pitch).

F.3. UAV Autonomous Navigation:

We observe that the UAV fails if the track has very sharp turns. This makes intuitive sense and the results that were produced by our BBGAN consistently produce such tracks. For the tracks that are only parameterized by three control points it is difficult to achieve sharp turns. However, our BBGAN is still able to make the UAV agent fail by placing the racing gates very close to each other, thereby increasing the probability of hitting them.

G. Training data

In the following we show some examples of the training data for each of the applications. Please refer to Figure 20 for some sample images of the object detection dataset. Figure 21 shows the training data used for the self-driving car experiments. Figure 24 shows some samples from the dataset used for the UAV racing application.

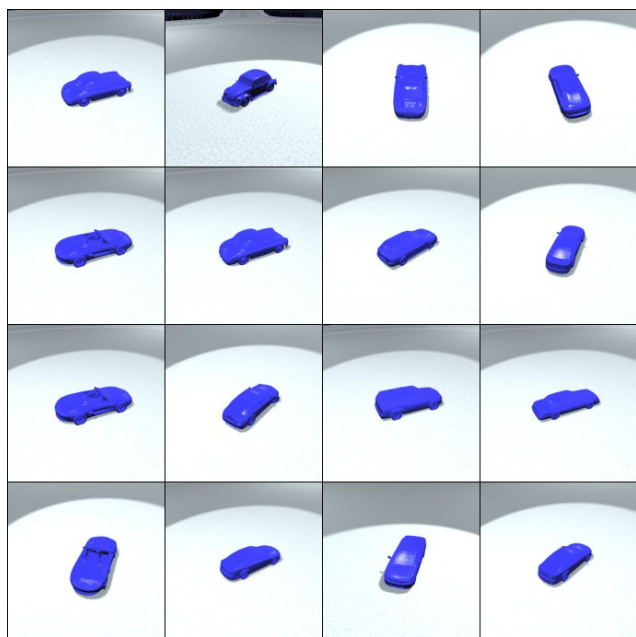


Figure 7: **Scenario 1 Qualitative Examples:** generated by BB-GAN

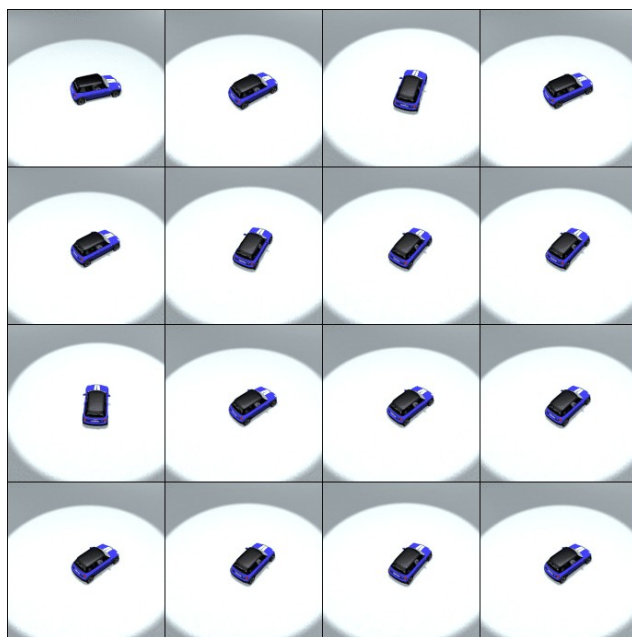


Figure 9: **Scenario 3 Qualitative Examples:** generated by BB-GAN

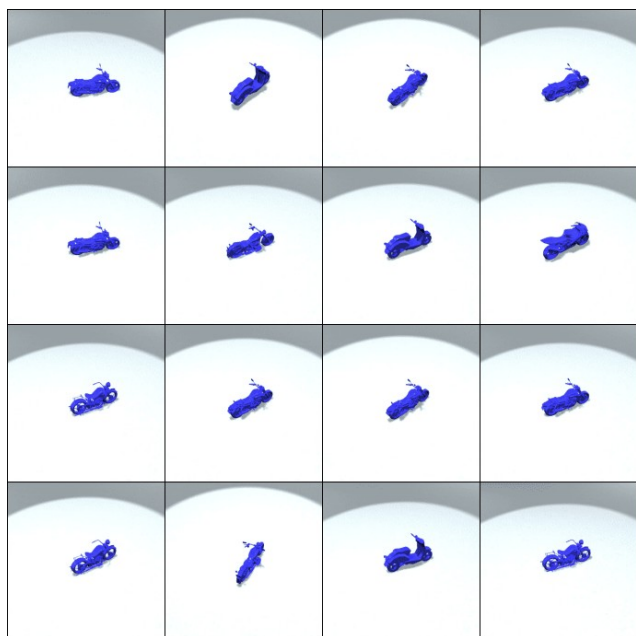


Figure 8: **Scenario 2 Qualitative Examples:** generated by BB-GAN

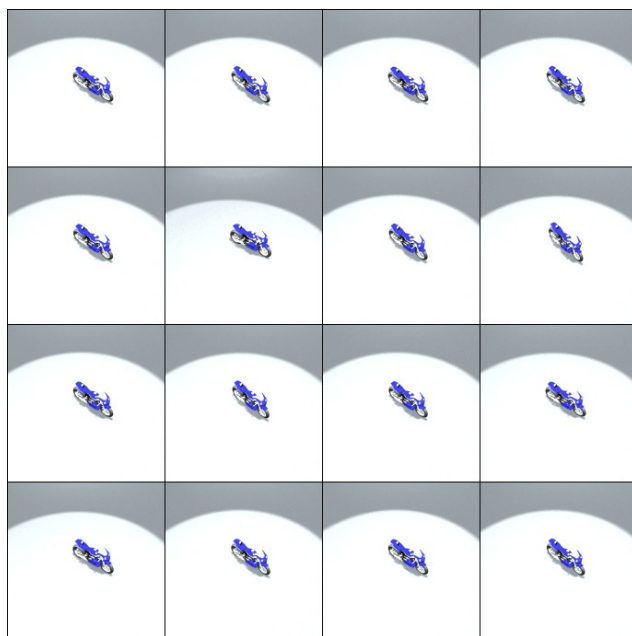


Figure 10: **Scenario 4 Qualitative Examples:** generated by BB-GAN

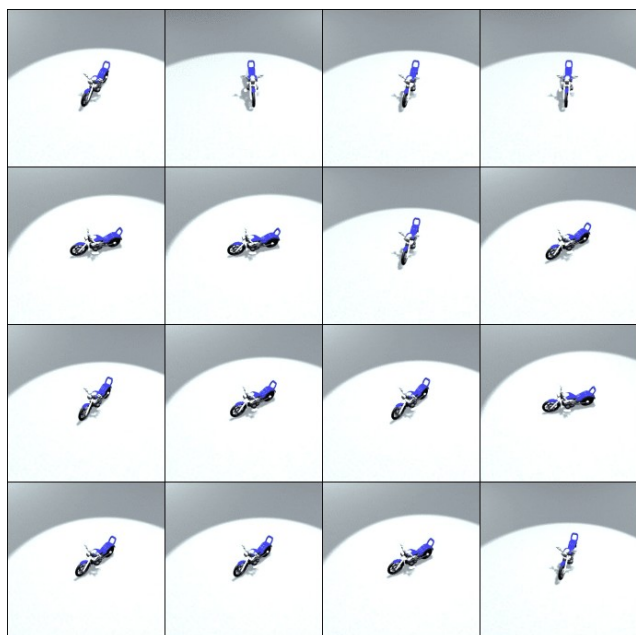


Figure 11: **Scenario 5 Qualitative Examples:** generated by BB-GAN

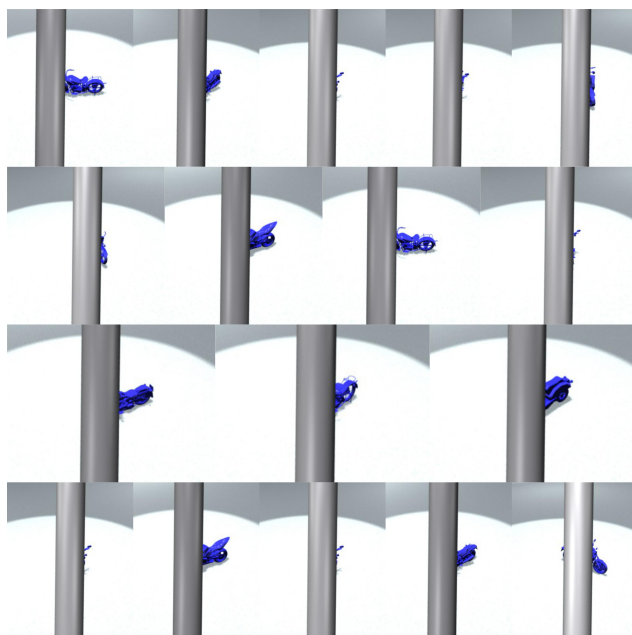


Figure 13: **Scenario 7 Qualitative Examples:** generated by BB-GAN

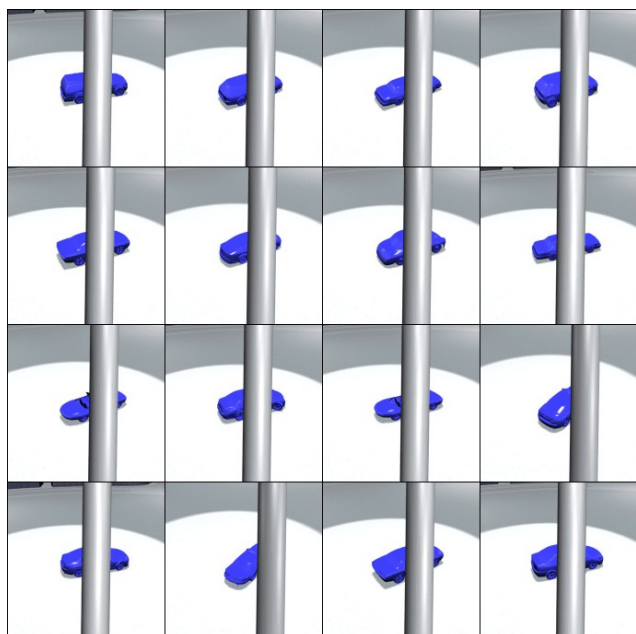


Figure 12: **Scenario 6 Qualitative Examples:** generated by BB-GAN



Figure 14: **Scenario 8 Qualitative Examples:** generated by BB-GAN

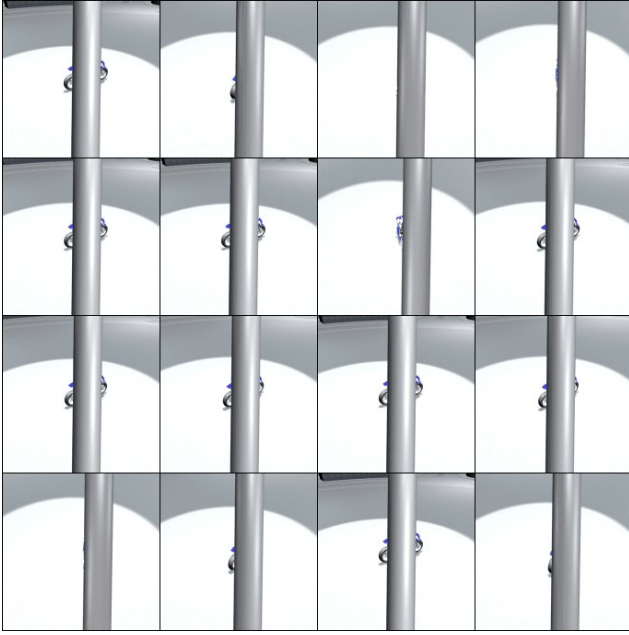


Figure 15: **Scenario 9 Qualitative Examples:** generated by BBGAN

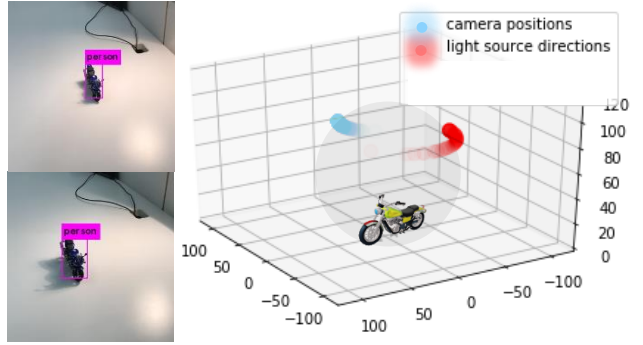


Figure 17: **Visualization of the fooling distribution.** In one analysis scenario above, we fix object to be a motorbike and fix the distance to the camera. We train a BBGAN to learn the fooling camera and light source angles to fool the YOLO detector. We plot the camera positions and light source directions of 250 sampled parameters in a 3D sphere around the object. On the left we show how taking real images from these angles confuses the YOLOV3 detector as well.

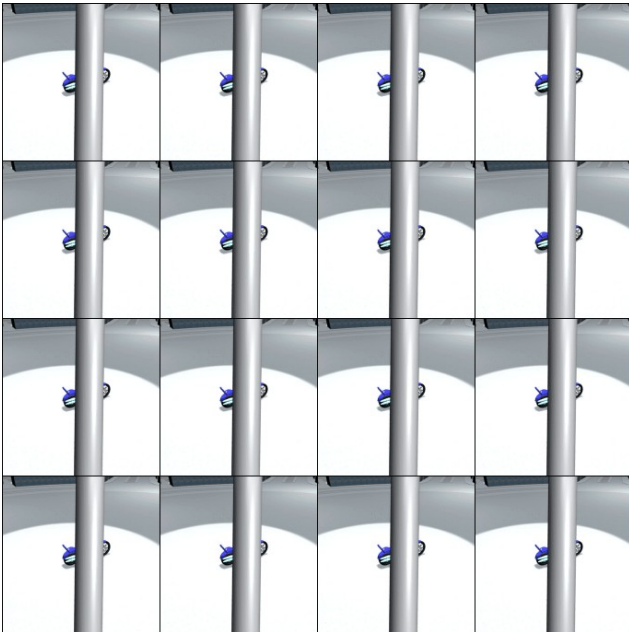


Figure 16: **Scenario 10 Qualitative Examples:** generated by BBGAN

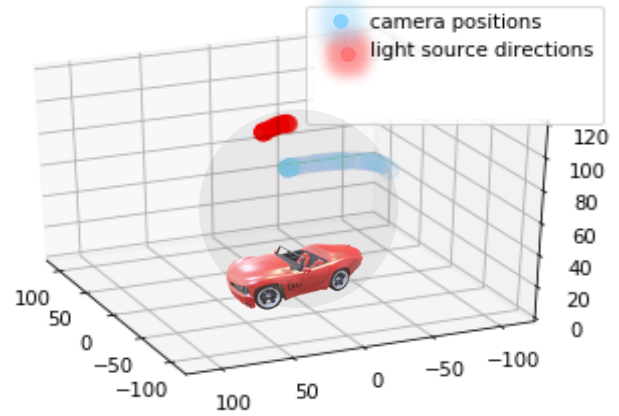


Figure 18: **Visualization of the fooling distribution.** In one analysis scenario above, we fix object to be a car and fix the distance to the camera. We train a BBGAN to learn the fooling camera and light source angles to fool the YOLO detector. We plot the camera positions and light source directions of 250 sampled parameters in a 3D sphere around the object.

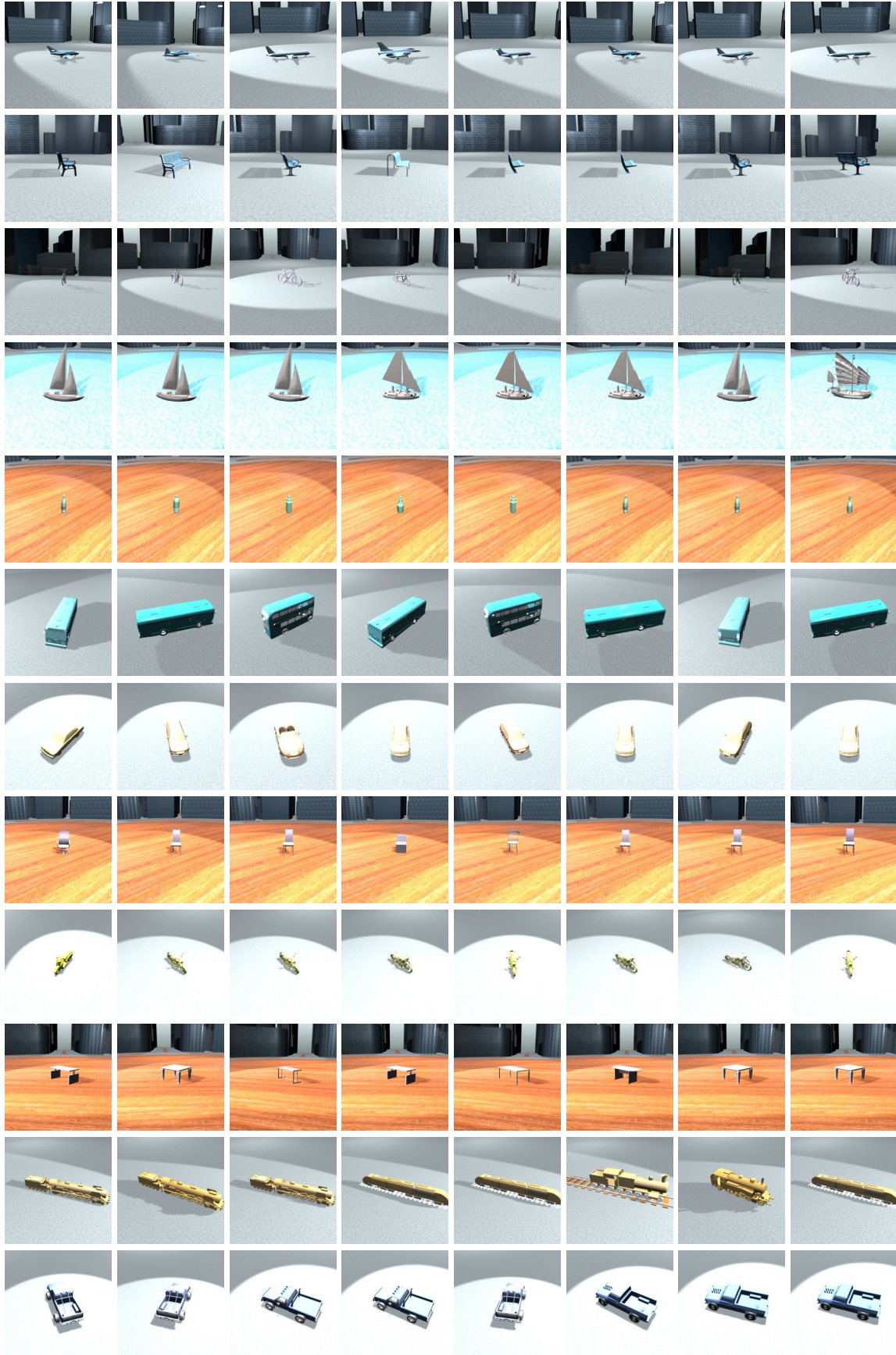


Figure 19: **Object detection** - Some sample images for each class that were rendered according to parameters generated by BBGAN which fooled the object detector.



Figure 20: **Object detection** - Some sample images from the dataset used for object detection with YOLOv3. Note that in the actual dataset each object has a random color regardless of its class. For clarity we uniformly color each class in this figure.

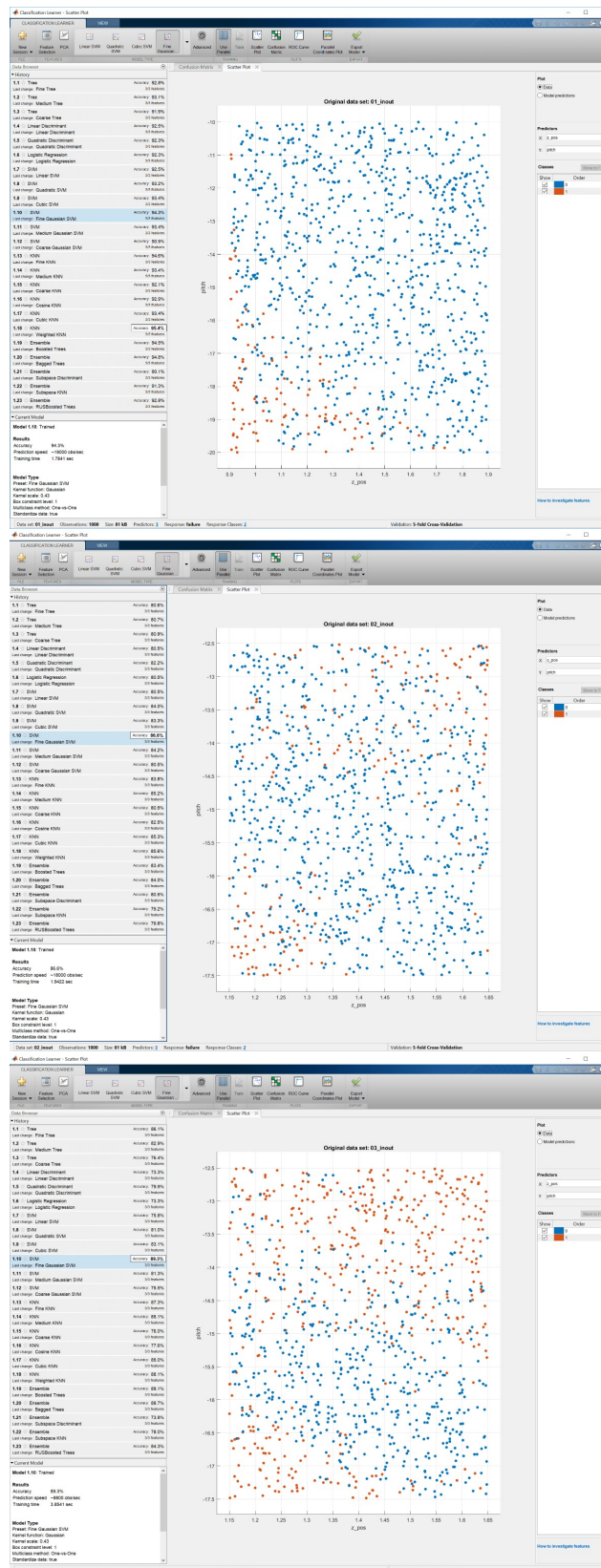


Figure 21: **Self-driving** - Visualization of training data distribution.

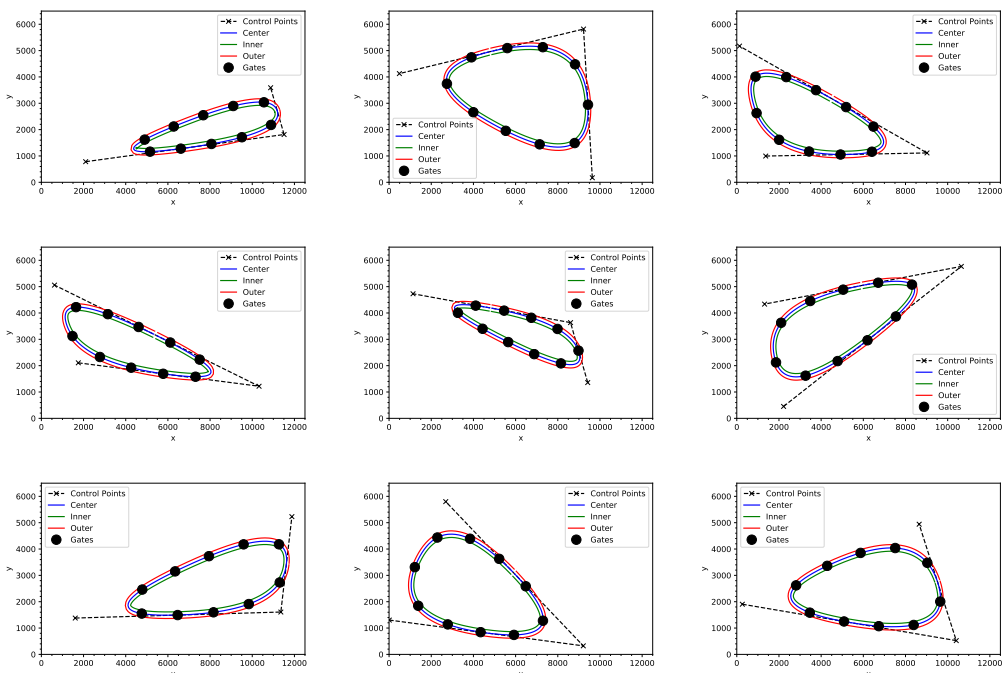


Figure 22: UAV racing - Some sample tracks from the dataset with 3 control points.

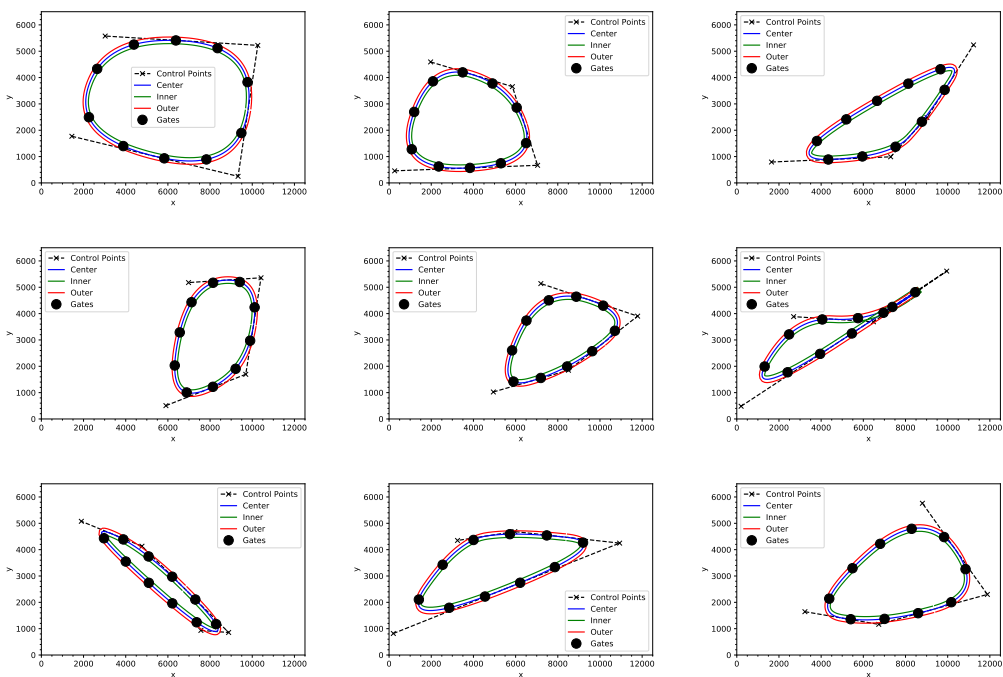


Figure 23: UAV racing - Some sample tracks from the dataset with 4 control points.

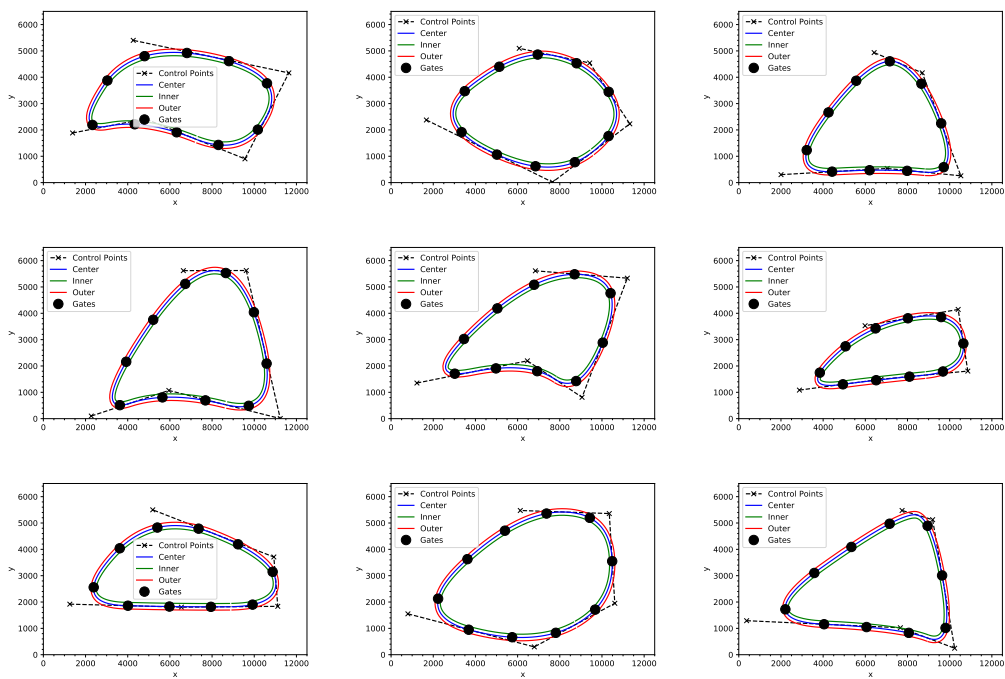


Figure 24: UAV racing - Some sample tracks from the dataset with 5 control points.